THREE-DIMENSIONAL FLOW IN A TRANSONIC AXIAL FLOW FAN OF A HIGH BYPASS RATIO TURBOFAN ENGINE

A.F. ABD EL-AZIM[1]   M.H. GOBRAN[2]   H.Z. HASSAN[3]

ABSTRACT

The present study deals with the air flow through an axial flow transonic fan blades, found in high bypass turbofan engines. Examples are CF-6, RB211 and GE90 turbofan engines. The fan has a wide chord, highly twisted blades of large span with a mean hub-to-tip ratio of about 0.404. The blades are tapered with its maximum chord at the tip radius. Moreover, these twisted blades have slight reduction in its maximum thickness from hub to tip.   Consequently, the flow field is a three dimensional viscous compressible. The engine intake together with the fan resemble the case studied here. The computational domain includes two periodic merged sectors at a central angle of 360 degrees divided by the number of blades (38). The first sector is stationary, which represents the intake domain, while the second is rotating, which represents the fan domain that comprehending one blade. This is an effective way of reducing the calculation time and speeding up the iterations. The investigated model (Intake and fan blade) dimensions and configuration are identified by measuring real dimensions of CF-6 engine fan module. The FLUENT solver employing the Spalart-Allmaras turbulence model is used to solve the flow field in both the intake and fan. The program results represent the variation of the flow characteristics (pressure, temperature, Mach number,............, etc) in the flow field at the design condition (cruise conditions; namely, 11000 m altitude, 0.85 Mach number and 3674 rpm fan speed). The fan performance map was also predicted for a range of percentage fan corrected speed from 60% to 110%.

KEY WORDS

Transonic flow, Axial fan, High bypass turbofan engine, Intake, swept blades.

---

[1] Professor, [2]Assistant professor and [3]Demonstrator, Mechanical Power Engineering Department, Zagazig University.
1) dr_ahmedhelal@yahoo.com.

INTRODUCTION

In advanced turbofan engines, the demand for greater power, minimum size and weight, reduced fuel consumption, specified pollutant emission and noise level, high reliability and low operation and maintenance costs is required. The fan in a commercial or military turbofan engine is a critical component to the successful attainment of the performance and efficiency targets of the entire engine. Fan efficiency directly affects specific fuel consumption of the engine. Any improvement in the fan efficiency has a strong influence on the engine thermal efficiency, and any shortfall in capacity is detrimental to the overall propulsion system efficiency. As a result, modern high bypass turbofan engines employ a highly-loaded, low-aspect ratio fan stage with transonic or low-supersonic relative velocities in the blade-tip region. The tip-section airfoils of these fan blades are noticeably different from the airfoil sections on the rest of the blade. The airfoils have a sharp leading edge that makes them prone to flow separation at off-design conditions. Due to extreme flight envelope requirements, the engines are often operated near the stall flutter boundary of the fan. At these conditions the fan tip section is subjected to high incidence angles and high transonic or supersonic relative Mach numbers. Blade flutter and associated high cycle fatigue problems result. These are very detrimental to the engine service life and must be avoided. Interest in the flow through fan blades has increased in recent years. Since the fan has large blade heights and highly twisted blades, the flow through it is very complicated and can be considered as a three dimensional one. Then the 3D-Navier-Stokes equations are necessary for describing the flow field. Such a three-dimensional Navier-Stokes computations of transonic fan flow using an explicit flow solver and an implicit $k - \varepsilon$ solver were introduced by Jennions and Turner [1]. They used the $k - \varepsilon$ model with wall function, and the radial equilibrium condition has been applied at the exit boundary. The fan simulations presented were chosen to demonstrate the flow pattern in three cases, an isolated rotor (NASA rotor 67), both the rotor and stator rows together at the design point (GE/Wennerstrom rotor 4), and the real engine of the NASA / GE E3 fan including the part span shroud. All simulations yielded good results compared with experimental data and showed that CFD has matured into a technology useful for industrial design.

A comparison of the measured and calculated flow field in a modern fan-bypass configuration was conducted by Goyal and Dawes [2]. In their study, the three dimensional viscous Navier-Stokes flow solver of Dawes was used. The turbulent viscous stresses are computed using the Bladwin-Lomax mixing length model. Results of the analysis were compared with experimental data. They found that, the predicted efficiency exceeded the measured value by about two and half percent. The trend of the predicted fan characteristics was in good agreement with the testing results. Even with the relatively simple tip clearance model used in calculations, the predicted tip clearance effects agreed well with the observed data.

Turner and Jennions [3] compared between the accuracy of two turbulence models, using some experimental data as a reference. One of them was the Bladwin-Lomax algebraic model, while the other was the $k - \varepsilon$ model. The used code had been

applied to the solution of the flow in a transonic fan rotor. They found that, the flow rate in the $k - \varepsilon$ solution is closer to experiment than the Bladwin-Lomax solutions.

Advanced research was conducted to design a swept wide chord fan blade with a high specific flow value (mass flow rate per unit area) at aero design point. This design has several potential benefits; namely, lower noise levels and higher thrust force than conventional engines having the same fan diameter. Such an advanced design concept is presented by Falchetti, Quiniou, and Verdier [4], and Beiler and Carolus [5], who introduced an aerodynamic design of such swept blades, high specific flow and wide chord fan. The major objective of this design was to prove the aerodynamic feasibility of a large increase in fan specific flow, with a minimum fan diameter for a given flow rate. Their preliminary design of Snecma Ts31 swept wide chord fan blade demonstrated the feasibility of increasing the inlet specific flow of commercial fans with good aerodynamic performance. The design objectives were matched by combining the benefits of wide chord technology and both axial and tangential sweep of the blade. They proved that, the wide chord technology and both axial and tangential sweep of the blade fulfilled the structural design requirements as well as the aerodynamic design objectives. Moreover, they indicated that, for fans that have a small potential of specific flow increase, there is a potential of 5 to10 % increase in the fan specific flow. Hence, up to 5% saving in fan diameter is expected for a given mass flow.

In this paper the flow through a highly-twisted transonic fan, installed in a high bypass turbofan engine, is investigated at the design condition and the fan performance map is predicted.

MATHEMATICAL MODELING

The 3D-Navier-Stokes equations are necessary for describing the flow field. Some assumptions are needed here. The first level of assumptions leads to the Reynolds-averaged Navier-Stokes equations. These are obtained by time averaging for the variables in these equations. This filters out the turbulence or random fluctuations of the flow field. The dependent variables in these equations then become the unsteady deterministic (non-random) velocity, energy, and density. Apparent stresses are produced by the averaging process due to the time unsteadiness of the actual flow field and the nonlinear terms in the equations. The problem with this system of equations is how to determine these apparent stresses and close the system. This is accomplished by assuming a suitable turbulence model. Such Reynolds-averaged Navier-Stokes equations require a model for the turbulent shear stresses. The Boussinesq hypothesis may be used, which defines an effective turbulent shear stress as the strain multiplied by the turbulent viscosity.

The flow governing equations; namely, conservation of mass, momentum, and energy equations, as well as some other auxiliary fundamental equations will be introduced. These basic equations are expressed in a fixed frame of reference. That

they are based on the absolute velocity formulation over the whole domain. The continuity, momentum and energy equations are expressed, respectively, as follows:

$$\frac{\partial}{\partial x_i}(\rho \overline{V_i}) = 0 \tag{1}$$

$$\frac{\partial}{\partial x_j}(\rho \overline{V_i}\,\overline{V_j}) = -\frac{\partial \overline{p}}{\partial x_i} + \frac{\partial}{\partial x_j}\left[\mu_{eff}\left(\frac{\partial \overline{V_i}}{\partial x_j} + \frac{\partial \overline{V_j}}{\partial x_i} - \frac{2}{3}\delta_{ij}\frac{\partial \overline{V_l}}{\partial x_l}\right)\right] \tag{2}$$

$$\frac{\partial}{\partial x_i}\left[\overline{V_i}(\rho E + \overline{p})\right] = \frac{\partial}{\partial x_i}\left[K_{eff}\frac{\partial \overline{T}}{\partial x_j} + \overline{V_i}(\tau_{ij})_{eff}\right] \tag{3}$$

where the over bar indicates time averaged variables.

The effective viscosity μ_{eff} is the sum of the laminar and turbulent viscosities and is given by:

$$\mu_{eff} = \mu + \mu_t$$

and the effective conductivity K_{eff} is the sum of the laminar and the turbulent thermal conductivities, and is given by:

$$K_{eff} = K + K_t$$

The stress tensor $(\tau_{ij})_{eff}$ is calculated using effective viscosity μ_{eff}, and is given by:

$$(\tau_{ij})_{eff} = \mu_{eff}\left(\frac{\partial \overline{V_j}}{\partial x_i} + \frac{\partial \overline{V_i}}{\partial x_j}\right) - \frac{2}{3}\mu_{eff}\frac{\partial \overline{V_i}}{\partial x_i}\delta_{ij} \tag{4}$$

The auxiliary fundamental equations are the equation of state, Sutherland viscosity law, and the isentropic relations describing the relation between the total or relative total conditions and the static ones in terms of the absolute or relative Mach number.

The Spalart-Allmaras Model of Turbulence

The evaluation of the performance of the fan blades also requires an accurate prediction of the turbulent boundary layer and of a possible separation of the blade boundary layer. Therefore it was decided to use the Spalart-Allmaras model of turbulence which is known to be one of the best turbulence models for the prediction of fan aerodynamics and includes a good low-Reynolds-number model [6]. The Spalart-Allmaras model is relatively simple one-equation model that solves modeled transport equations for the kinematic turbulent viscosity. This model was designed specifically for aerospace applications involving wall-bounded flows and has been shown to give good

results for boundary layers subjected to adverse pressure gradients. It is also gaining popularity for turbomachinery applications. The Boussinesq hypothesis is used in the Spalart-Allmaras model of turbulence. The advantage of this approach is the relatively low computational cost associated with the computation of the turbulent viscosity μ_t.

The model proposed by Spalart and Allmaras [7] solves a transport equation for a quantity that is a modified form of the turbulent kinetic viscosity. The transported variable in the Spalart-Allmaras model, $\tilde{v}$, is identical to turbulent kinematic viscosity except in the near-wall region. The transported equation for $\tilde{v}$ is :

$$\frac{\partial}{\partial x_i}(\rho \tilde{v} V_i) = G_v + \frac{1}{\sigma_{\tilde{v}}}\left[\frac{\partial}{\partial x_j}\left((\mu + \rho\tilde{v})\frac{\partial \tilde{v}}{\partial x_j}\right) + C_{b2}\rho\left(\frac{\partial \tilde{v}}{\partial x_j}\right)^2\right] - Y_v \tag{5}$$

Where;

G_v: production of turbulent viscosity.

Y_v: destruction of turbulent viscosity that occurs in the near-wall region due to wall blocking and viscous damping.

v: molecular kinematic viscosity.

$\sigma_{\tilde{v}}, C_{b2}$: are constants.

CASE STUDY

The case study examined represents a subsonic intake followed by an axial flow fan. This fan is installed on a high bypass ratio turbofan engine like the GENERAL ELECTRIC CF6-50. The fan rotor has a tip diameter of 2.183 m with tapered, highly twisted blades. The blade heights are 0.682 m and 0.619 m at inlet and outlet, respectively (the mean blade height is 65.05 cm) . The mean hub to tip ratio is 0.404.

It was very difficult to get sufficient and accurate specifications of such a fan and its intake in the literature, and the engine manual. So the fan and the intake detailed dimensions were measured from the real fan model of the CF6-50 turbofan engine at the maintenance workshop of the Egypt Air Company. The airfoil section dimensions and stagger angles were measured at four different locations through the blade height; namely, the hub, the tip, and two other intermediate sections. These sections help in drawing the overall blade profile, that shown in figure (1). Figure (2) illustrates the fan blade profile while table (1) gives some important dimensions of the four sections.

A detailed dimensions of the intake and fan are shown in figure (3). The axial length of the intake was found to be 155.55 cm, and the nose of the fan can be approximated as a hemisphere of radius 40.75 cm.
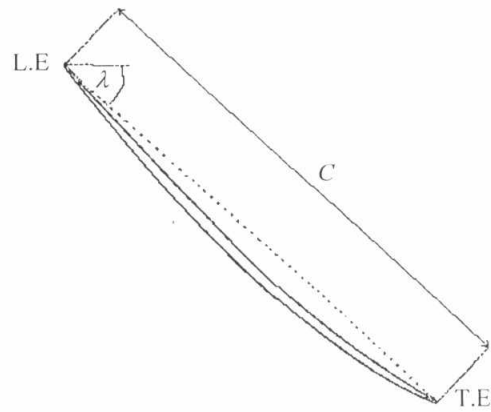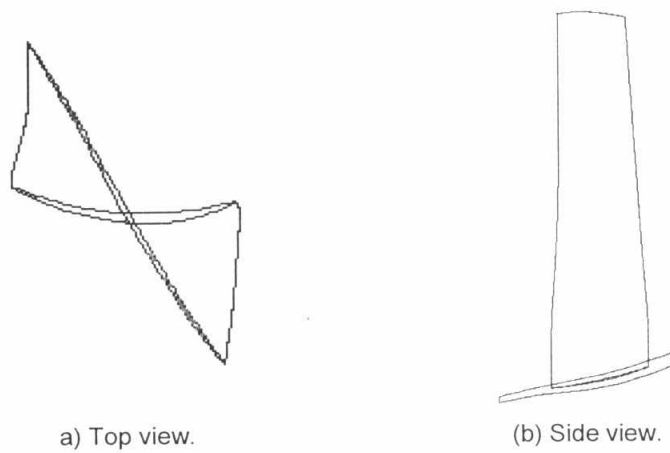
Figure (1): Typical fan blade section.

| a) Top view. | (b) Side view. |

Figure (2): Fan blade profile.

Table (1): Blade dimensions and stagger angles at different sections through the blade height

	Hub section. $r = 43.98$ cm	Section at $r = 69.0$ cm.	Section at $r = 89.0$ cm.	Tip section. $r = 109.05$ cm.
Chord length C	17.5 cm.	19.4 cm.	21.5 cm.	24.4 cm.
Stagger angle λ	$10.0°$.	$43°$.	$49°$.	$66°$.
Location of max. thickness %C (measured from the blade leading edge).	65.71	58	48.15	47.8
Max. thickness mm.	9	7.5	4.2	3.71
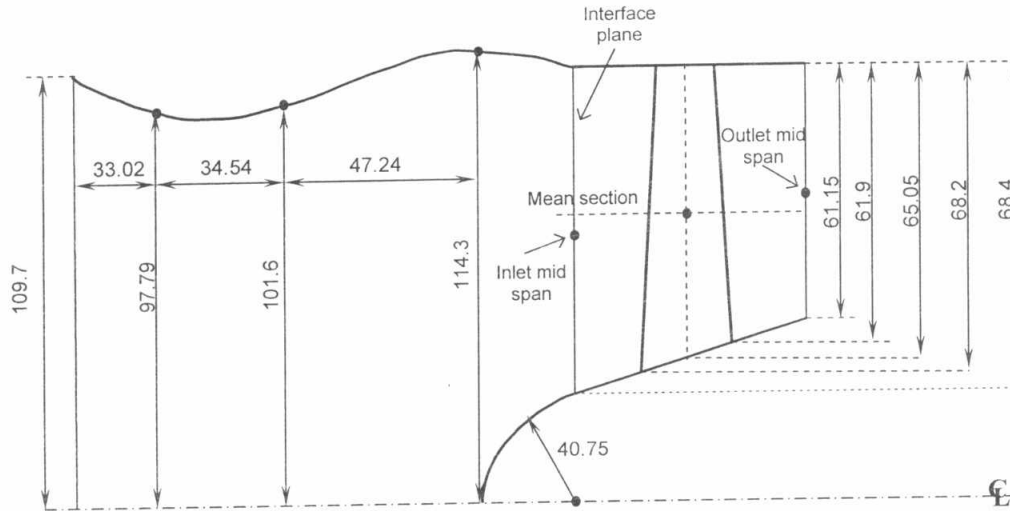
Figure (3): Detailed dimensions of the intake and fan (all dimensions in cm).

NUMERICAL MODEL

The computational domain in the study includes both of the fan and the intake zones. Due to the large dimensions of both the intake and the fan combination, it was very difficult to solve the overall domain. Since the fan includes 38 similar blades, a periodic sector of a central angle of (360/38) was generated separately for both the fan and the intake zones. The two zones were merged together to form the required computational domain. The fan passage was adjusted automatically in a manner that makes the flow tangent to the blade at both inlet and exit of the fan. This is shown in the figure (4).
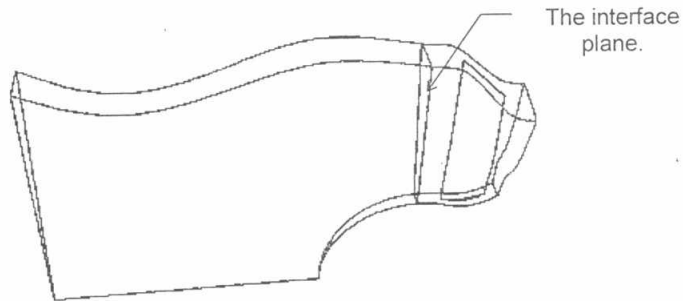
Figure(4): The domain of the solution.

MESH GENERATION:

The GAMBIT preprocessor (a part of the FLUENT package) is used to construct the geometry of the solution domain for both the intake and fan zones. It is also used to generate the suitable mesh. The mesh of both the fan and the intake zones are generated and stored separately into two mesh files. The two meshes are merged using the TMERGE utility in the FLUENT package. Due to complex geometry of both the fan and intake sectors, it is suitable to use the unstructured tetrahedral grid. To facilitate the meshing of the fan zone, it is divided into three spanwise sections. The mesh in each spanwise section is generated separately. The grid is refined near and at all walls of the two zones (intake and fan) in order to permit accurate near-wall treatment of the turbulence model. Figures (5-a) and (5-b) show the grids over a blade-to-blade surface at the tip and the hub sections, respectively. Table (2) summarizes the mesh characteristics on the whole domain.

Table (2): Grid characteristics.

	Intake block	Fan block	All the domain
Number of cells	49005	281941	330946
Number of faces	99020	585640	692844
Number of nodes	11353	59403	72011
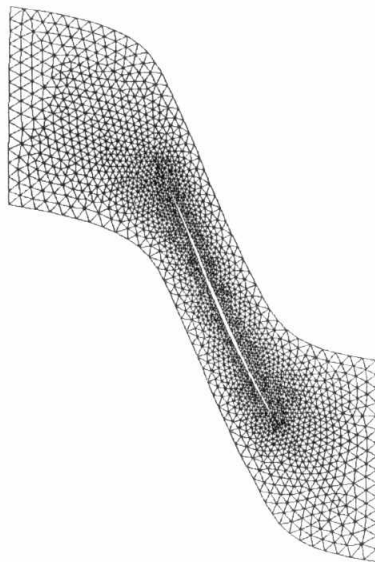
Figure (5-a): The mesh at the tip section.   Figure (5-b): The mesh at the hub section.
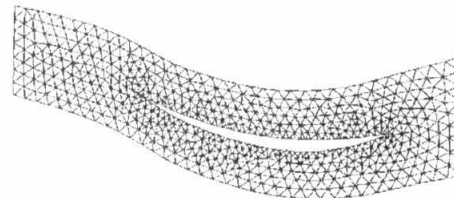
NUMERICAL TECHNIQUE:

The previous mathematical model is solved in this study using the commercial code Fluent 6.1. This code is a general purpose computer program for modeling fluid flow, heat transfer and chemical reactions. Fluent solves the governing integral equations for the conservation of mass, momentum, energy, and turbulence using a control-volume-based technique.

The segregated solver was selected to solve the flow domain where, the governing equations are solved sequentially (i.e., segregated from one to another). Each iteration consists of the steps outlined below [8]:

1. Fluid properties are initialized and successively updated, based on the current solution.
2. The momentum equation are solved in turn using current values for pressure and face mass fluxes, in order to update the velocity field.
3. Since the velocities obtained in Step 2 may not satisfy the continuity equation locally, an equation for the pressure correction is derived from the continuity equation and the linearized momentum equations. This pressure correction equation is then solved to obtain the necessary corrections to the pressure and velocity fields and the face mass fluxes such that continuity is satisfied.
4. Equations for scalar quantities such as turbulence, and energy are solved using the previously updated values of the other variables.
5. A check for convergence of the equation set is made (the convergence criterion requires that the residuals decrease to 10^{-3} for all equations except the energy equation, for which the criterion is 10^{-6}).

RESULTS

The contours of Mach number at three sections of the intake are illustrated in figure (6). The Mach number is maximum near the casing and decrease in the radially inward direction upstream the fan nose; figure (6-a). Then it reverse its behavior for sections (b and c) where its maximum value is near the nose.

Figures (7-a) through (7-e) illustrate the radial variation of the flow properties (relative Mach number, static and total pressures, and static and total temperatures). Two lines or curves are shown to demonstrate the air properties upstream and downstream of the fan.

To illustrate variation of the flow field properties along various blade-to-blade surfaces over the fan blade span, the relative Mach number, relative total pressure, total and static pressures and temperatures are calculated and plotted in figures (8) through

(13) for five blade sections. These blade sections are at the blade hub, tip, and a quarter, half and three quarters of the blade span.

Figure (8-a) illustrates the relative Mach number near the root. The constant relative Mach number contours show a rapid acceleration over the suction side near the leading edge. The relative Mach number is then reduced in the rearward direction on both surfaces. Similar pattern dominates for 25% of span, and mean sections. It is noticed that over the mean section some points acquired sonic speeds or a little bit higher. Transonic velocities are dominated over more than one third of the suction surface.

In figure (8-d) and (8-e) captured normal shocks are seen near the trailing edge of the suction surface. The flow over the tip section is completely supersonic over the suction side and subsonic flow is found in small regions in the passage downstream the section trailing edge. Over the pressure side, the relative Mach number is also supersonic over one third or even more of the chord. Then the flow crosses the normal shock wave propagating from the suction's trailing edge. Thus over the remaining section of the pressure surface, the flow is subsonic.

The relative total pressure is illustrated in figures (9-a) to (9-e). At the hub section the relative total pressure is nearly constant which resembles the minimum value over the blade span. Moving radially outward, for 25% span, densed contours for the relative total pressure is shown near the leading edge over the suction side and the maximum value is over the pressure surface. At the mean section a further rise in the total pressure is noticed with a cluster of pressure lines near the leading edge which attains its maximum value also near the pressure surface. Over the 75% span and tip sections, the shock waves previously mentioned is clearly shown. The relative total pressure across the normal shock wave is noticeably reduced (from 96 kPa to 88 kPa at tip section).

Figure (10-a) to (10-e) illustrates the total pressure contours over the five sections of the fan. Similar patterns to fig(9) are seen. However, the contours are widely spaced with little clustering near the blade leading edge. Over the 75% span and tip sections the normal shock wave is also clearly noticed. Same for figures (11) , (12), and (13) representing the contours of static pressure, total and static temperature respectively. These variables increase in the downstream direction for the five sections. For the 75% span as well as tip sections, the shock wave formed at the trailing edge of the suction surface propagating towards the opposite pressure side of the next blade is identified by clustered contours and sudden rise in these operating variables.

The fan map is shown in figure (14) for different rotational speeds varying from 60% to 110% of the design value. The map closely represents the typical axial flow compressor (fan) behavior where the range of the relative corrected mass flow rate is reduced with the increase of the rotational speed. The surge line as well as the cruise condition operating line are drawn. Figure (15) shows the efficiency lines for the same variable relative corrected speeds. The code developed by Gobran [9] is used to obtain the fan operating line. This is done by matching between the components of the high

bypass turbofan engine (CF6), where the developed fan characteristics is introduced to this code. It is noticed that, at the design speed and pressure ratio, there is slight deviations between the efficiency (about 1.27%) and mass flow rate (about 10%) compared with those listed in the engine manual. Moreover, computations revealed that at the design speed, approximately 10.5% stall margin remained beyond design pressure ratio.

CONCLUSIONS

1- Numerical solution for the flow field across the fan of a high bypass ratio turbofan engine is presented here using the commercial code FLUENT. The flow field is treated as 3D viscous flow, where the Spalart-Allmaras turbulence model is employed.

2- The studied model represents a subsonic intake followed by an axial flow fan. This fan is installed on a high bypass ratio turbofan engine. The fan rotor has a tip diameter of 2.183 m with tapered, highly twisted wide chord blades. The blade heights are 0.682 m and 0.619 m at inlet and outlet, respectively. The mean hub to tip ratio is 0.404. A periodic sector of a central angle of (360/38) is generated separately for both the fan and the intake zones. The two zones are merged together to form the required computational domain. The GAMBIT preprocessor is used to construct the geometry of the solution domain for both the intake and fan zones. It is also used to generate an appropriate mesh that contains 330946 cell for the whole domain.

3- The absolute Mach number in the intake decreases successively in the direction towards the fan. The computations clarifies that upstream of the fan nose the maximum Mach number increases in the radially outward direction. For sections along the nose this Mach increase has reversed its direction to be in the radially inward direction.

4- The air flow properties are plotted over 5 successive blade-to-blade surfaces at the hub, mean, and tip as well as 25% and 75% span.

5- The relative Mach number reaches and exceeds unity over the outer part of the blade (from nearly 55% of the blade span up to its tip section).

6- Shock waves are formed at the trailing edge of the suction side of each blade propagating towards the pressure side of the opposite blade for the outer quarter of blade. This is accompanied by rise in static and total pressures as well as static and total temperatures. The relative total pressure is decreased.

7- The fan map is also drawn over a range of speed lines varying from 60% to 110% of the design value. Moreover, the surge line and the operating line at cruise conditions are also plotted on the fan map. The efficiency curves for each speed are plotted as well for the same relative speeds.
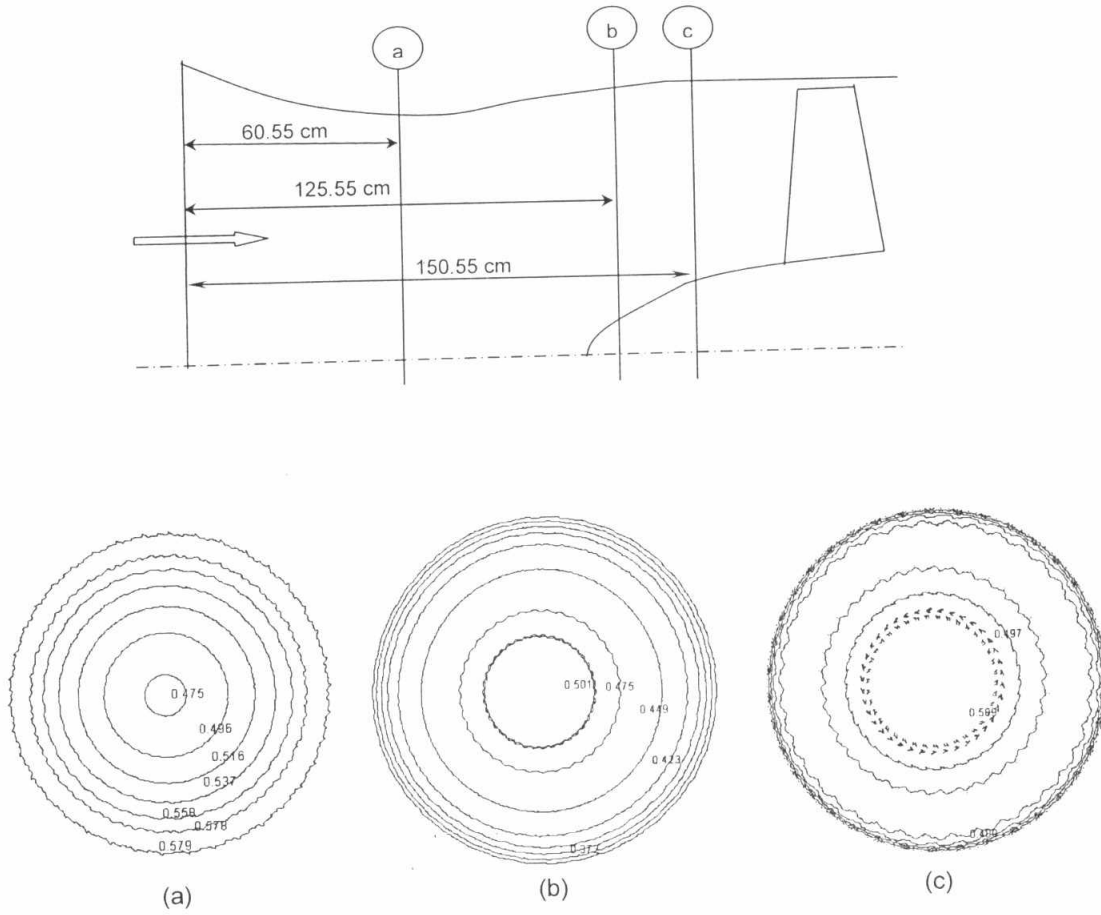
Figure (6) sections at different axial distances in the intake.
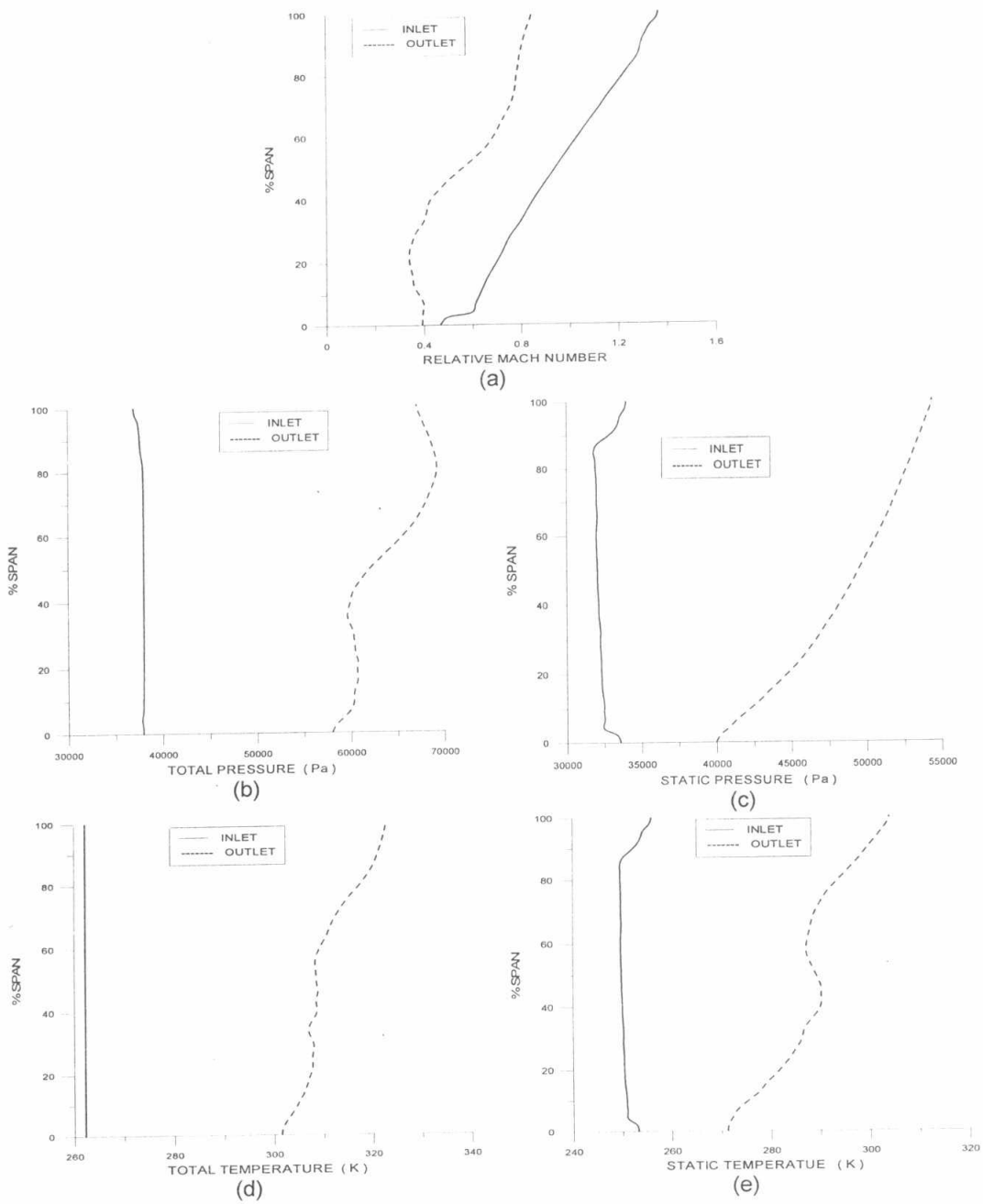
Figure (7): Radial variations of the flow conditions at inlet and outlet of the fan.

a) At the hub section

b) At 25% span from the hub section

c) At the mean section

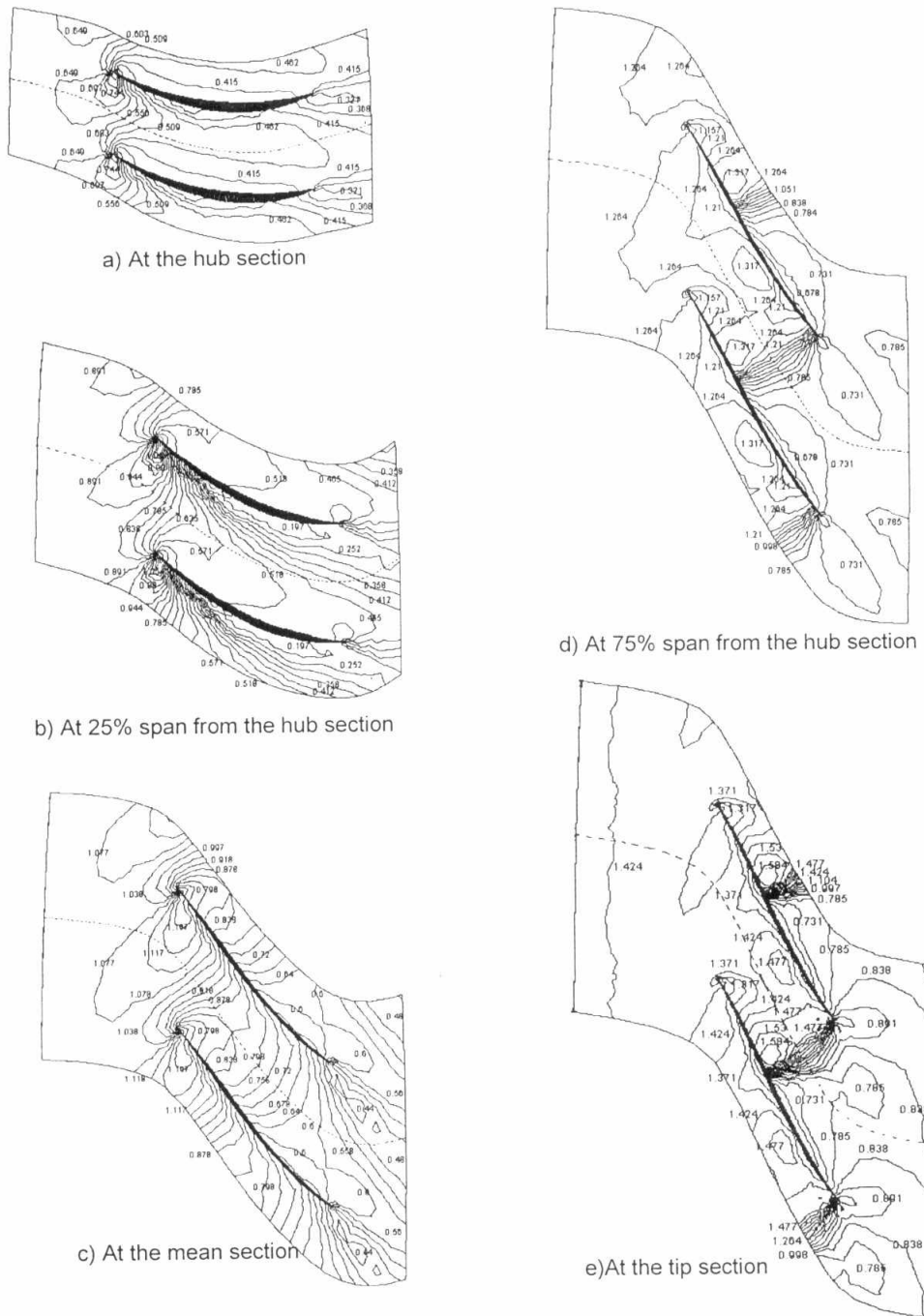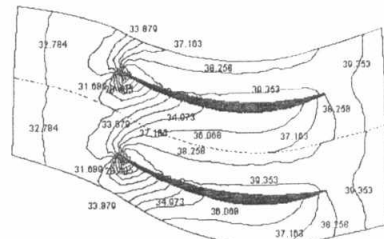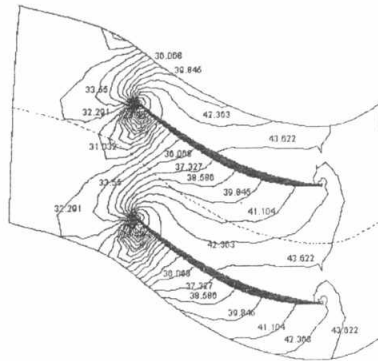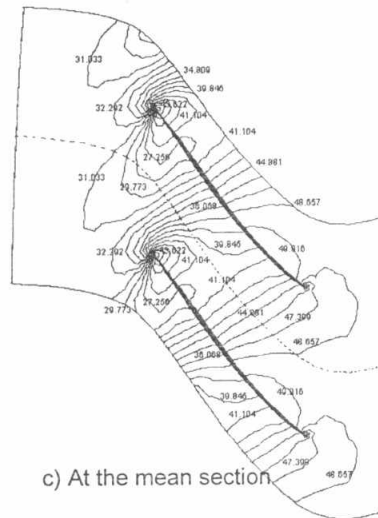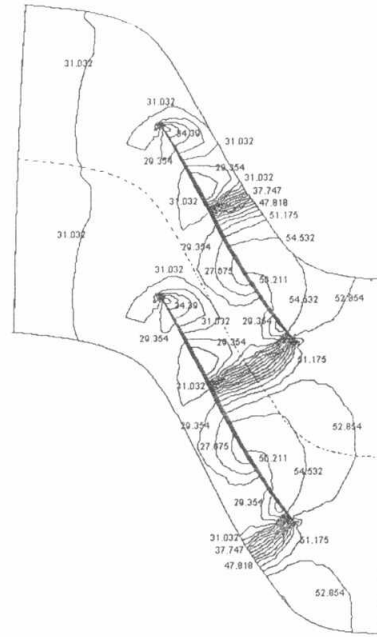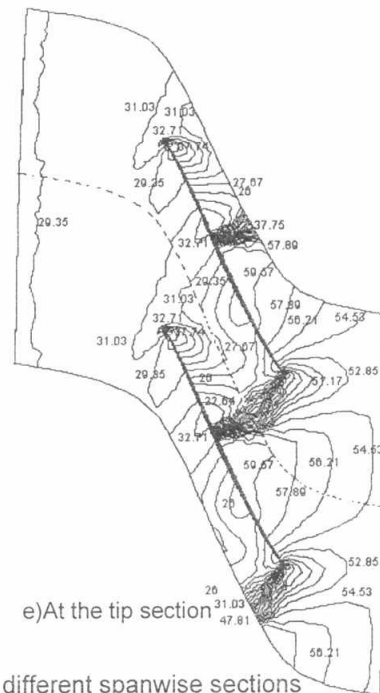d) At 75% span from the hub section

e)At the tip section

Figure (8) : Contours of relative Mach number at different spanwise sections

a) At the hub section

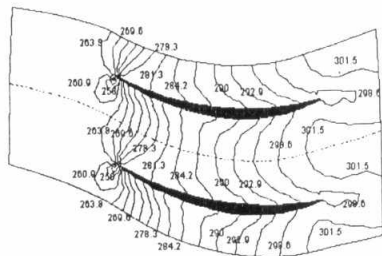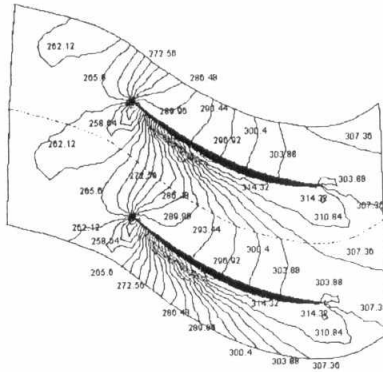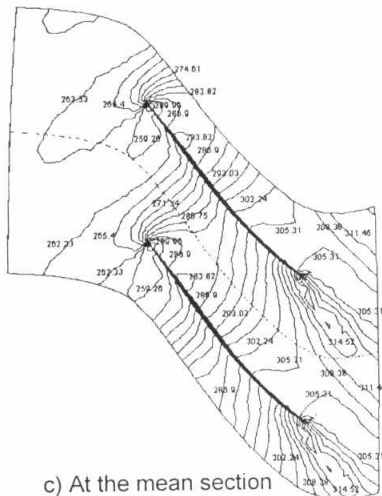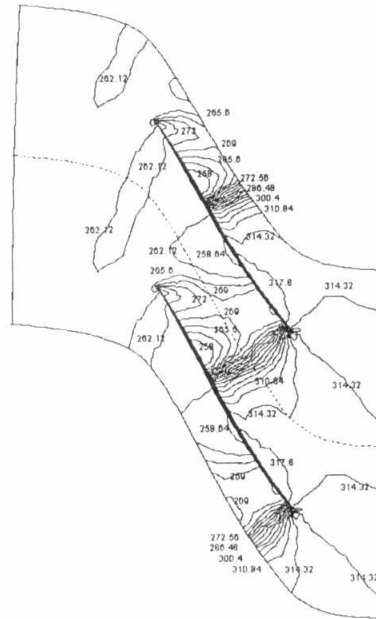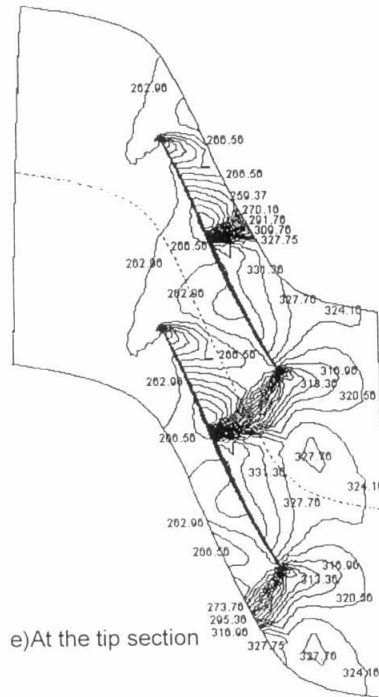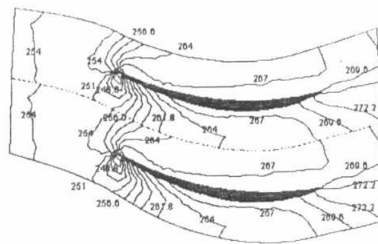b) At 25% span from the hub section

c) At the mean section

d) At 75% span from the hub section

e) At the tip section

Figure (9) : Contours of relative total pressure at different spanwise sections

a) At the hub section

b) At 25% span from the hub section

c) At the mean section

d) At 75% span from the hub section
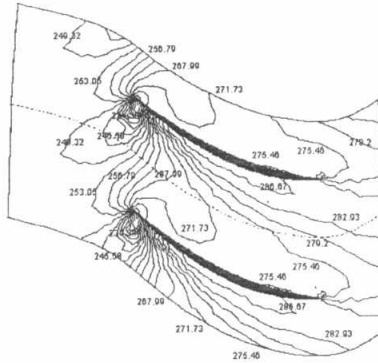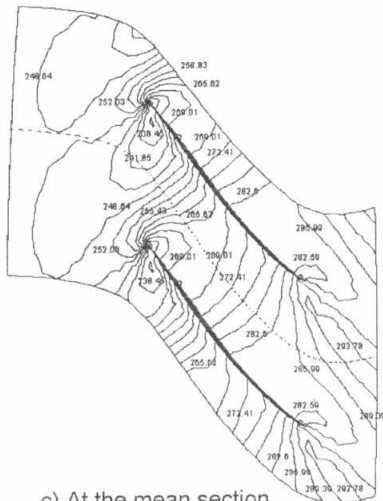

e) At the tip section

Figure (10) : Contours of total pressure at different spanwise sections

a) At the hub section

b) At 25% span from the hub section

c) At the mean section

d) At 75% span from the hub section

e) At the tip section

Figure (11) : Contours of static pressure at different spanwise sections

a) At the hub section

b) At 25% span from the hub section

c) At the mean section

d) At 75% span from the hub section

e) At the tip section

Figure (12) : Contours of total temperature at different spanwise sections
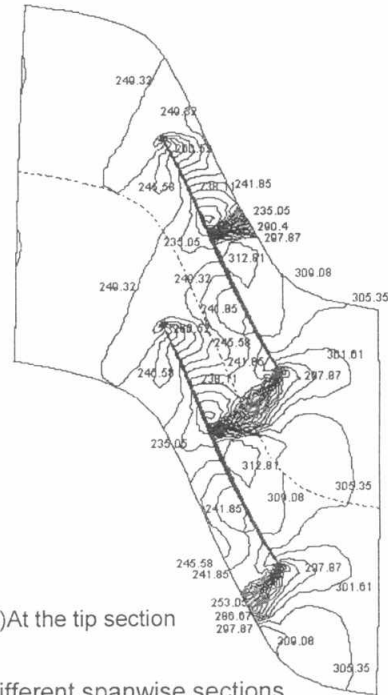
a) At the hub section

b) At 25% span from the hub section

c) At the mean section
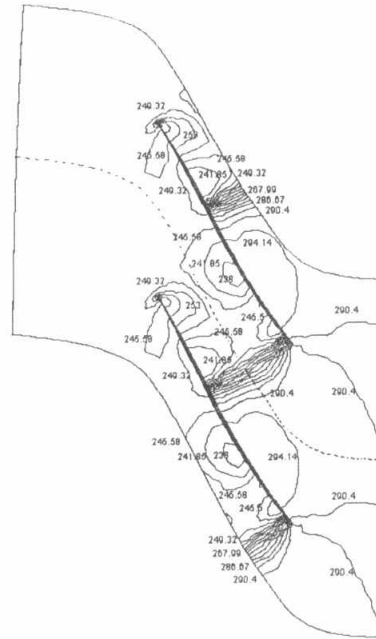
d) At 75% span from the hub section

e) At the tip section

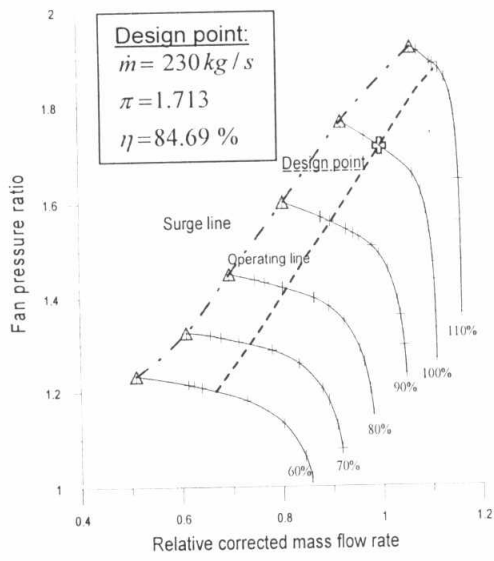Figure (13) : Contours of static temperature at different spanwise sections
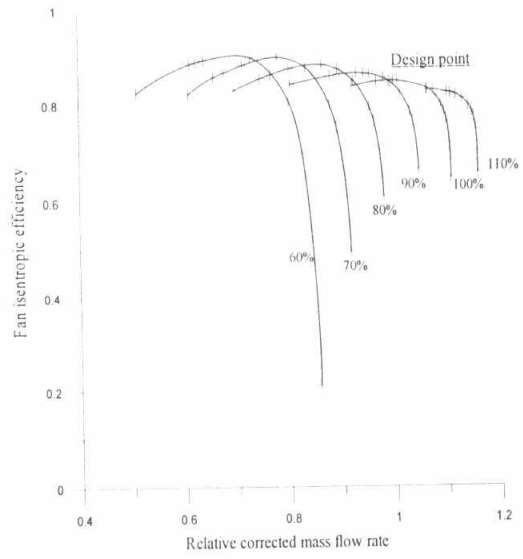
Figure (14) Fan map.

Figure (15) Fan efficiency.

REFERENCES

[1] Jennions,I.K. and Turner, M. G. "Three-Dimensional Navier-Stokes Computation Of Transonic Fan Flow Using An Explicit Flow Solver And An Implicit $k - \varepsilon$ Solver", journal of turbomachinery, ASME Transactions, April 1993, Vol. 115

[2] Goyal, R. K. And Dawes W. N. "A Comparison Of The Measured And Predicted Flow Field In A Modern Fan-Bypass Configuration.", journal of turbomachinery, ASME Transactions, vol. 115, April 1993.

[3] Turner, M. G. and Jennions, I. K. "An Investigation Of Turbulence Modeling In Transonic Fans Including A Novel Implementation Of An Implicit $k - \varepsilon$ Turbulence Model", journal of turbomachinery, ASME Transactions, April 1993, vol. 115.

[4] Falchetti, F. Quiniou, H. and Verdier L. "Aerodynamic Design And 3d Navier-Stokes Analysis Of A High Specific Flow Fan", Presented at the international gas turbine and aeroengine congress, The Hague, Netherlands, June 13-16, 1994.

[5] Beiler, M. G. and Carolus T. H. " Computation And Measurement Of The Flow In Axial Flow Fans With Skewed Blades.", Journal of turbomachinery, ASME Transactions, 1999, Vol. 121.

[6] Tschirner, T. , Pfitzner, M. , and Merz, R. " Aerodynamic Optimization Of An Aeroengine Bypass Duct OGV-Pylon Configuration.", proceeding of ASME Turbo EXPO 2002.

[7] Spalart, P. and Allmaras, S. "A One-Equation Turbulence Model For Aerodynamic Flows." Technical Report AIAA-92-0439, American Institute of Aeronautics and Astronautics, 1992.

[8] Fluent 6.1 Documentation (User Guide Manual).

[9] Gobran, M.H. "Analytical Approach To Turbofan Engine Modeling, Control And Non-Linear Simulation." Ph. D. Thesis, Cairo university, 1995.